Scilight

Journal of Hazards, Risk and Resilience
https://www.sciltp.com/journals/jhrr



Article

Check for updates

Decadal Reconstruction of Monsoon Flood Inundation in the Kabul River Basin Using Sentinel-1 SAR and Machine Learning

Zahid Ur Rahman [1,2]

[1] International Research Center of Big Data for Sustainable Development Goals (CBAS), Beijing 100094, China; 31192048@mails.ucas.ac.cn
[2] University of Chinese Academy of Sciences, Beijing 100094, China

How To Cite: Rahman, Z.U. Decadal Reconstruction of Monsoon Flood Inundation in the Kabul River Basin Using Sentinel-1 SAR and Machine Learning. *Journal of Hazards, Risk and Resilience* **2026**, *1*(1), 25. https://doi.org/10.53941/jhrr.2026.100025

Received: 29 June 2026
Revised: 18 August 2026
Accepted: 10 September 2026
Published: 29 September 2026

Abstract: Flood inundation mapping in mountainous basins remains challenging because of complex terrain, frequent cloud cover, and limited ground observations. This study reconstructs monsoon flood inundation in the Kabul River Basin (KRB) during 2015–2025 using Sentinel-1 Synthetic Aperture Radar (SAR) and a Random Forest (RF) machine-learning framework. A multi-feature dataset comprising pre- and post-flood VV and VH backscatter, polarization metrics, GLCM texture descriptors, and topographic variables was developed, while high-confidence pseudo-labels were used for event-specific RF classification. The results reveal substantial interannual variability in flood extent, with the largest inundation recorded in 2020 (1004 km^2), followed by high flood extents in 2021 and 2022. Except for 2017, monsoon-related inundations were detected in every year, and the cumulative inundated area exceeded 4000 km^2, with flooding predominantly concentrated in downstream lowland areas. The RF framework achieved overall accuracies of 0.86–0.93, Cohen's Kappa values of 0.78–0.86, and an integrated ROC-AUC of 0.924. These findings demonstrate the utility of Sentinel-1 SAR and RF for consistent reconstruction of historical monsoon inundation in data-scarce mountainous basins and provide a temporally consistent flood inventory for hydrological analysis and subsequent flood-susceptibility assessment.

Keywords: Sentinel-1 SAR; machine learning; flood inundation mapping; monsoon floods; Kabul River Basin

1. Introduction

Flooding remains one of the most destructive hydrological hazards worldwide, causing substantial economic losses, agricultural damage, and human displacement, particularly in regions characterized by rapid population growth and hydro-climatic variability [1,2]. Mountain river systems are especially vulnerable due to steep terrain, short concentration times, and the interaction of extreme rainfall with snowmelt processes [3]. The KRB, located in the eastern Hindukush Mountain range and extending across Afghanistan and Pakistan, exemplifies these challenges [4]. The basin experiences intense monsoonal rainfall, episodic cloudburst events, and glacier-melt contributions that collectively generate complex flood regimes, including fluvial and flash flooding [5]. Increasing climatic variability and expanding settlement along river corridors have heightened exposure and vulnerability, underscoring the need for reliable reconstruction of historical flood inundation.

Accurate delineation of flood inundation is essential for hydrological assessment, model calibration, and flood susceptibility assessment [6]. Optical remote sensing has traditionally been used for flood detection; however, persistent cloud cover during monsoon periods often limits its applicability [7]. SAR, particularly

Copyright: © 2026 by the authors. This is an open access article under the terms and conditions of the Creative Commons Attribution (CC BY) license (https://creativecommons.org/licenses/by/4.0/).
Publisher's Note: Scilight stays neutral with regard to jurisdictional claims in published maps and institutional affiliations.

Sentinel-1, provides all-weather, day-night observations and has become a primary tool for operational flood monitoring [6,8]. Floodwater typically reduces radar backscatter due to specular reflection over smooth water surfaces, enabling event-based change detection approaches [9,10].

Despite these advantages, SAR-based flood mapping in mountainous basins is complicated by terrain-induced distortions, variability in incidence angle, vegetation structure, and heterogeneous land cover [11]. Conventional threshold-based change detection, where inundation is identified by fixed reductions in backscatter between pre and post-flood event scenes, can be sensitive to local radiometric conditions and may produce false positives over steep slopes or rough surfaces [2,7]. Such approaches may also lack consistency when applied across multiple events with varying acquisition geometries and hydro-meteorological conditions.

Recent studies have demonstrated the complementary value of optical and microwave Earth-observation data, as well as cloud-based processing, for flood inundation monitoring. Multi-source satellite approaches have improved flood detection across heterogeneous image conditions by transferring information between different pre- and post-event observations [12], while cloud-computing platforms such as Google Earth Engine (GEE) have enabled rapid flood delineation from Sentinel-1 imagery using change-detection and automatic-threshold approaches [13]. Regional applications over the Ghaggar River Basin and Kerala have further demonstrated the effectiveness of Sentinel-1 SAR for rapid flood mapping under monsoon conditions and highlighted the importance of precipitation, elevation, and slope in interpreting inundation patterns [13]. Recent multiscale flood-risk research has also demonstrated the value of combining climatic indicators with satellite-based flood observations to characterize disaster impacts across different spatial scales [14]. At a broader scale, the use of a decade of Sentinel-1 observations has demonstrated the potential of long-term SAR archives for constructing consistent historical flood extents and identifying recurrent flood-prone areas [15]. These studies collectively highlight the advantages of multi-source observations, cloud-based processing, and long-term satellite archives for flood monitoring, while also demonstrating the need for consistent methods capable of handling heterogeneous terrain and repeated flood events.

To address these complications, machine learning techniques provide an alternative by modelling nonlinear relationships between radar features and flood occurrence. Random Forest (RF), an ensemble decision-tree algorithm introduced by Breiman [16], has demonstrated strong performance in remote sensing classification tasks due to its robustness to noise, resistance to overfitting, and ability to handle high-dimensional predictors. In SAR flood applications, RF has been shown to outperform single-threshold methods, particularly when incorporating multi-temporal backscatter, polarization features, and texture descriptors [10,17]. Texture metrics derived from Gray-Level Co-occurrence Matrices (GLCM) can improve discrimination between inundated vegetation and non-flooded rough terrain. Furthermore, the exclusion of permanent water bodies, using long-term surface water occurrence datasets, enhances flood-event specificity [18].

A persistent limitation in multi-event flood mapping is the availability of consistent reference data for supervised training. In transboundary basins such as the KRB, authoritative flood polygons are not uniformly available across years. Self-training or pseudo-label strategies, in which high-confidence flood and stable non-flood pixels are identified using conservative change criteria, provide a practical solution for constructing balanced training datasets while preserving methodological consistency over time [19,20].

In this study, we develop a Random Forest–based flood inundation mapping framework for major monsoon flood events in the KRB during 2015–2025. By applying a consistent machine learning framework across a decade of flood events, this study aims to (1) enhance the robustness of SAR-based flood delineation in mountainous hydrological systems, (2) reduce inter-event methodological bias associated with threshold approaches, and (3) generate a temporally consistent flood inventory to support hydrological analysis and flood susceptibility assessment in the KRB.

2. Study Area Description

The Kabul River Basin (KRB), located in the eastern Hindu Kush (EHK) region, is a transboundary basin shared by Afghanistan and Pakistan and forms a major tributary of the Indus River system [21]. The basin extends approximately between 33°40′–36°75′ N and 69°50′–73°50′ E, covering an area of about 57,675 km^2 [4]. It originates in the high mountains of the Hindu Kush and drains eastward, joining the Indus River near Attock, Pakistan [1]. For this study, a GIS-based watershed delineation approach was adopted using a consistent basin boundary to ensure spatial comparability in flood mapping and susceptibility analysis (Figure 1).

As shown in the study area map, topographically, the basin exhibits extreme relief, with elevations ranging from about 259 m to 7680 m above sea level. Slopes in the southeast region range from 0 degrees to 80 degrees in the northern highlands. The northern and northeastern regions are dominated by steep slopes, deep valleys, and

rugged mountainous terrain, while downstream areas transition into wider floodplains and low-gradient valley systems. This strong geomorphological contrast plays a key role in flood generation and propagation, with steep headwaters favoring rapid runoff and flash flooding, whereas downstream plains are more prone to fluvial inundation and urban flooding [22,23].

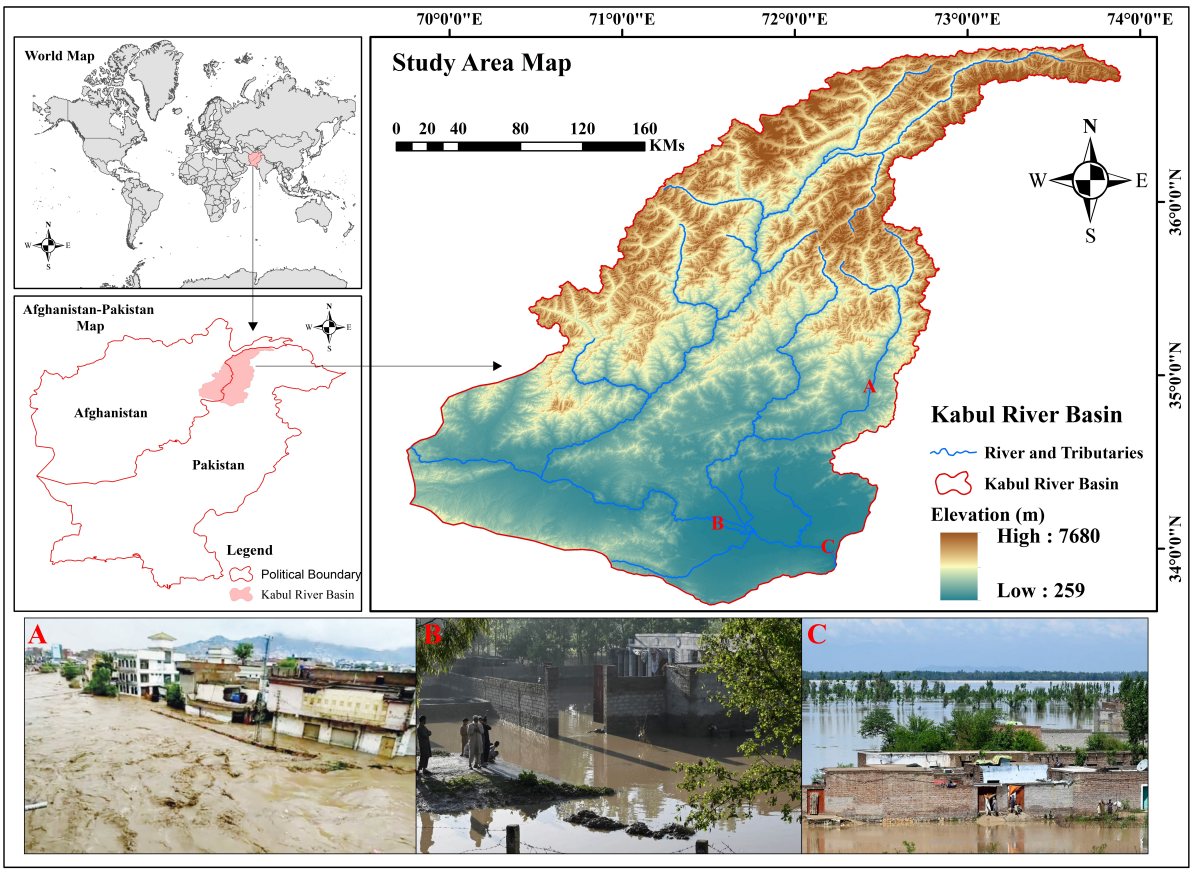


Figure 1. Study area map showing the locations affected by flooding during the study period: (**A**) Swat, (**B**) Peshawar, and (**C**) Nowshera.

Climatically, the KRB lies within a semi-arid to arid zone but experiences strong spatial variability due to complex terrain. Mean annual temperature is approximately 13 °C, while average annual precipitation is around 459 mm, increasing to about 600 mm in the northern highlands [3,24]. The basin is influenced by both mid-latitude westerly disturbances and the South Asian monsoon, resulting in pronounced seasonal hydro-climatic variability [25]. Hydrologically, streamflow is strongly regulated by both monsoon rainfall and cryospheric processes, including snowmelt and glacial melt, which significantly contribute to seasonal runoff and flood generation [1,26]. The basin contains extensive cryosphere resources, including glaciers and seasonal snow covering approximately 1650 km^2 and more than 1000 glacial lakes, mainly concentrated in the upper sub-basins [3,22].

Land use in the basin reflects elevation-driven gradients, ranging from sparse vegetation in high mountains to agricultural and urban landscapes in valley floors. Major urban centers include Jalalabad, Swat, Peshawar, and Nowshera, where rapid urban expansion has increased impervious surfaces and flood exposure. Socioeconomically, the basin supports a population of over 22 million, with increasing growth rates on both sides of the border, intensifying pressure on flood-prone areas and critical infrastructure [27–29].

3. Materials and Methods

Historical flood inundation extents were mapped for major monsoon-driven flood events during 2015–2025 to provide objective evidence for constructing flood inventories used to train and validate the general and multi-type Flood Susceptibility assessment. Because threshold-based SAR change detection can be sensitive to scene-specific radiometry, acquisition geometry, and land cover heterogeneity, flood delineation was performed using a supervised Random Forest classification framework implemented in Google Earth Engine (GEE). The approach integrates multi-temporal Sentinel-1 backscatter features with texture and terrain descriptors and outputs event-specific flood probability and binary inundation maps for each flood window (Figure 2).

3.1. Overview of Machine Learning-Based Flood Mapping Framework

Flood inundation was mapped using an event-based, pre/post comparison strategy, in which Sentinel-1 composites were generated for each flood-event time window. Instead of applying a single fixed threshold to the backscatter difference image, a Random Forest classifier was trained for each event using high-confidence pseudo-labels (self-training seeds) to represent the flooded and non-flooded classes. This design reduces dependence on arbitrary thresholds and allows the model to learn nonlinear relationships between inundation and SAR signatures, particularly in complex environments such as mixed vegetation, rough floodwater, and settlements.

To enhance physical realism and minimize false positives, the workflow removed or minimized known confounders in SAR flood mapping, including: (i) acquisition geometry inconsistencies by using a single orbit pass, (ii) border noise and invalid edges in GRD products, (iii) permanent water bodies, and (iv) steep terrain prone to radar distortions and physically implausible flooding. These steps follow established SAR processing recommendations for Sentinel-1 GRD and flood applications.

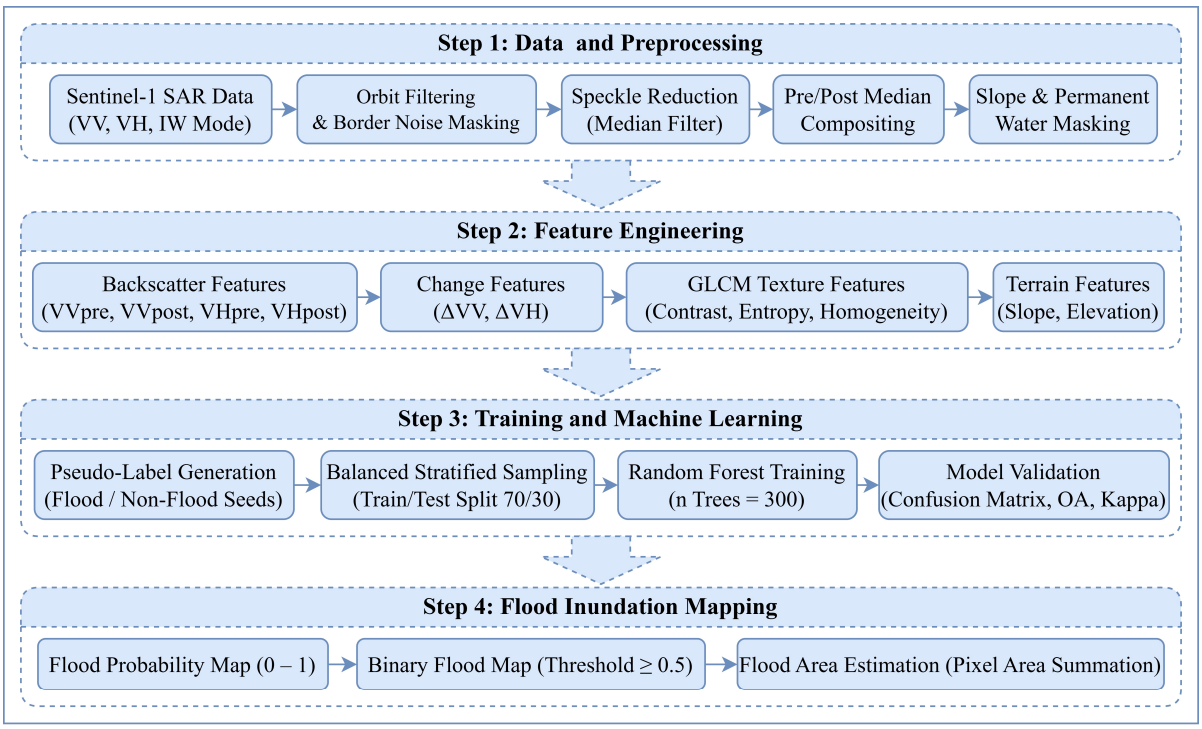


Figure 2. Methodological workflow of the flood inundation mapping using synthetic aperture radar and random forest classifier techniques.

3.2. SAR Image Selection and Preprocessing

For each flood event, Sentinel-1 GRD scenes were acquired for pre-flood and post-flood periods selected to capture (i) representative non-flood baseline conditions and (ii) peak or near-peak inundation conditions. The following rules were applied consistently across 2015–2025:

(1) Temporal proximity to flood timing: Pre-flood and post-flood composites were constructed from acquisitions close to reported flood dates to reduce land surface change unrelated to flooding.
(2) Orbit-pass consistency: Only scenes from the same orbit pass were used within each event to reduce incidence-angle and viewing-geometry effects on backscatter.
(3) Polarization availability: Both VV and VH polarizations were retained to capture complementary scattering responses associated with open water, inundated vegetation, and roughened surfaces.
(4) Artifact control: Scenes affected by pronounced GRD edge artifacts were mitigated through border-noise masking and incidence-angle constraints.

All Sentinel-1 processing was implemented in GEE. Scenes were filtered to IW mode and clipped to the basin boundary for consistent spatial support. To reduce speckle while preserving spatial patterns, each scene was smoothed using a focal median filter. Multiple scenes within each pre and post-flood time window were aggregated using a median composite, improving robustness against outliers and scene to scene noise.

To reduce the influence of edge artifacts in Sentinel-1 GRD products, a border-noise suppression mask was applied based on backscatter and incidence-angle constraints, consistent with operational recommendations to improve GRD quality.

A terrain constraint was applied using SRTM-derived slope to exclude pixels with slope exceeding a defined threshold (20°), where radar layover/shadow effects and physically implausible inundation are more likely in mountainous basins.

3.3. Feature Engineering and Confounding Factor Removal

For each event, a multi-source feature stack was created from the pre and post-flood Sentinel-1 composites (VV, VH, and incidence angle) combined with terrain descriptors. The feature set included:

(1) *Multi-temporal SAR backscatter and change metrics*

Pre- and post-event VV and VH backscatter bands were included directly (VVpre, VHpre, VVpost, VH_{post}). Change features were computed to highlight reductions in the water-related signal.

(2) *Polarimetric relation indicators*

To capture differential scattering between co- and cross-polarization, we derived polarization-difference features.

(3) *Textural features*

Because flooded surfaces and inundated vegetation can exhibit distinct spatial textures relative to non-flooded land cover, the Gray-Level Co-occurrence Matrix (GLCM) textures were extracted from post-flood VV imagery using a local window. Texture metrics included contrast, entropy, dissimilarity, and homogeneity. GLCM features with Random Forest have been shown to improve flood mapping performance, particularly in heterogeneous and mountainous settings.

(4) *Terrain covariates*

Shuttle Radar Topography Mission (SRTM) elevation and slope data were appended to reduce confusion from topographic distortions and to ensure the geomorphic plausibility of inundation pathways.

(5) *Permanent water exclusion*

Permanent water bodies were masked using the JRC Global Surface Water (GSW) occurrence product (occurrence ≥ 90%), ensuring the mapped inundation represents event-driven floodwater rather than stable lakes and reservoirs.

(6) *Slope masking*

Pixels above the slope threshold were excluded to minimize radar layover and shadowing and to avoid unrealistic flooding.

3.4. Training Data Generation and Model Implementation

Because event-specific ground-truth polygons are not consistently available across all years, training labels were generated using a conservative self-training (pseudo-label) strategy. Pixels were assigned as high-confidence flooded when they exhibited (i) strong positive ΔVV (indicating post-flood backscatter reduction) and (ii) low post-flood VV consistent with open water backscatter. Pixels were assigned as high-confidence non-flood when the change was near zero (stable surface), and post-flood VV was not water-like. All seed pixels were additionally constrained by slope and permanent-water masks. To prevent class imbalance, an equal number of flooded and non-flooded samples were drawn using stratified sampling, producing a balanced training dataset for each event.

A Random Forest classifier was trained for each event using the engineered feature stack. Random Forest constructs an ensemble of decision trees trained on bootstrapped samples; predictions are obtained by aggregating tree outputs. For a binary flood class, the RF class probability can be expressed as:

$$P(y = 1|x) = \frac{1}{K}\sum_{k=1}^{K} \mathbb{I}(T_k(x) = 1) \quad (1)$$

where x is the feature vector for a pixel, T_k is the k-th decision tree. K is the number of trees, and $\mathbb{I}(\cdot)$is the indicator function. The probability output $P(y = 1|x)$ was used to produce a continuous flood probability map (0–1). A binary flood inundation mask was then generated using a standard probability cutoff (0.5).

$$\hat{y} = \begin{cases} 1, P(y = 1|x) \geq 0.5 \\ 0, \ otherwise \end{cases} \quad (2)$$

3.5. Model Validation, Mapping, and Flood Area Estimation

For each event, the pseudo-labeled samples were randomly divided into 70% for training and 30% for testing. Overall accuracy and Cohen's Kappa were calculated from the held-out pseudo-labeled samples to assess the internal consistency of the RF classification relative to the high-confidence reference samples. Because these pseudo-labels were derived from Sentinel-1 backscatter characteristics, interpreting these metrics as internal classification-performance measures rather than fully independent estimates of map accuracy.

$$k = \frac{p_o - p_e}{1 - p_e} \tag{3}$$

where p_o is observed agreement and p_e is a chance agreement.

In addition, variable importance outputs from RF were examined to identify the most influential predictors (ΔVV, VV_{Post}, texture features), supporting interpretability and feature relevance. The flooded area was calculated by summing pixel area within the binary flood (A_{flood}) mask:

$$A_{flood} = \sum_{i=1}^{n} \hat{y}_i \cdot a_i \tag{4}$$

where, a_i is pixel area and $\hat{y}_i$ is the predicted flood label.

Event-specific probability and binary flood maps were exported and subsequently used to compile decade-scale flood evidence layers to support the development of flood inventories.

In addition to validation using labeled sampling for each year, the final integrated flood-inundation map is also validated using the flood inventory using the area under the curve (AUC) with ROC techniques.

4. Results

4.1. Flood Inundation Mapping

The results of the historical flood inundation analysis reveal significant year to year variability in flood-affected areas across the KRB during the monsoon period 2015–2025 (Figure 3). The total inundated area was estimated at approximately 420 km^2 in 2015, 379 km^2 in 2016, and 504 km^2 in 2018, indicating moderate floods during these years. In contrast, no flood inundation was observed in 2017, which is consistent with the absence of documented flood events in historical records for that year.

Flood severity increased markedly in subsequent years, with the largest flood extent recorded in 2020, when inundation covered approximately 1004 km^2 of the basin. This was followed by 2022, which experienced approximately 688 km^2 of flood-affected area, and 2021, with 624 km^2 inundated. In more recent years, the flood extent declined, with inundated areas of approximately 242 km^2 in 2023, 466 km^2 in 2024, and 459 km^2 in 2025. Among all assessed years, 2023 exhibited the lowest flood extent, highlighting the strong temporal variability in flood magnitude across the basin. Across the 2015–2025 period, a cumulative area of approximately 4008 km^2 was inundated at least once, indicating substantial spatial exposure to monsoon flooding across the basin. (Figure 4).

Overall, except in 2017, the basin experienced flood inundation every year between 2015 and 2025, underscoring the recurring nature of flood hazards in the KRB. Spatially, flood inundation was concentrated predominantly in the southern and downstream parts of the basin, where low-lying plains, gentle slopes, and dense river networks favor prolonged water retention. These geomorphological characteristics promote the formation of standing floodwater, which is effectively captured by Sentinel-1 SAR-based flood mapping techniques. The consistency between the SAR-derived flood extents and historical flood records further confirms the robustness of the inundation mapping approach and provides a solid foundation for developing reliable general and multi-type flood inventories for subsequent susceptibility analyses. It must be noted that this flood inundation represents only monsoon floods; the region also experienced pre-monsoon, spring, and winter floods.

4.2. Validation

The reliability of the flood inundation maps was evaluated using overall accuracy and Cohen's Kappa coefficient for each year between 2015 and 2025. The classification results demonstrate consistently strong performance throughout the study period. Overall accuracy values ranged between 0.86 and 0.93, while Kappa coefficients varied from 0.78 to 0.86. The classification results demonstrate consistent agreement with the held-out pseudo-labeled samples throughout the study period. Overall accuracy values ranged between 0.86 and 0.93, while Kappa coefficients varied from 0.78 to 0.86. These metrics indicate strong internal agreement between the RF predictions and the high-confidence pseudo-labels; however, because the pseudo-labels were generated from the same Sentinel-1-based feature space used for classification, they should not be interpreted as independent estimates of absolute mapping accuracy.

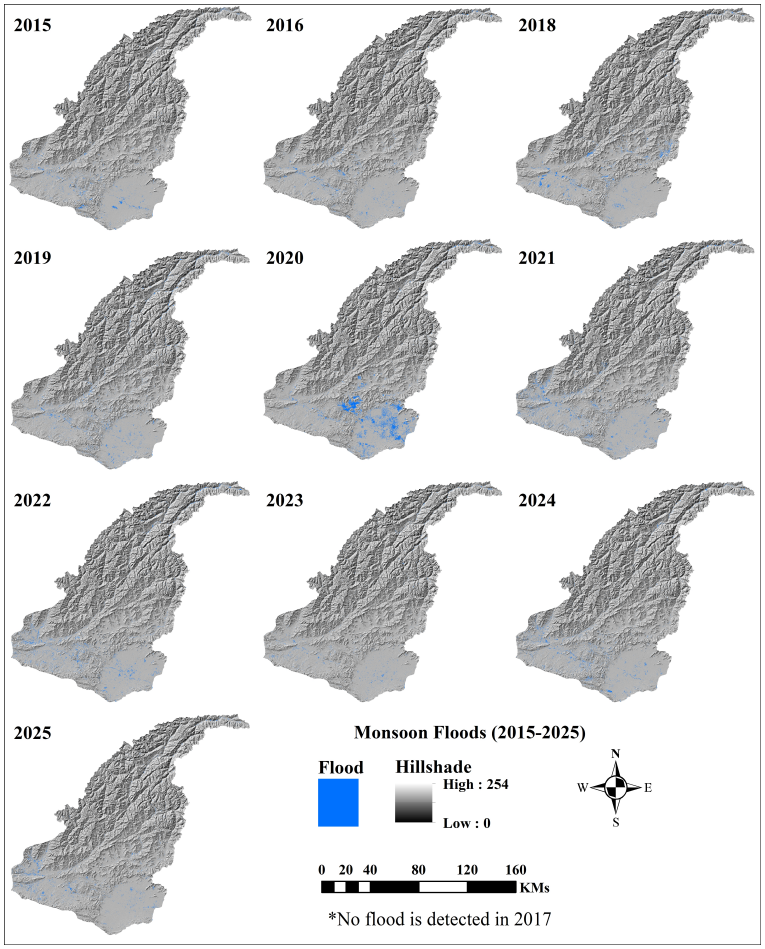


Figure 3. Monsoon flood distribution in the Kabul River Basin (2015–2025). Blue areas indicate flood-affected zones overlaid on hillshade; the integrated panel shows cumulative flood extent.

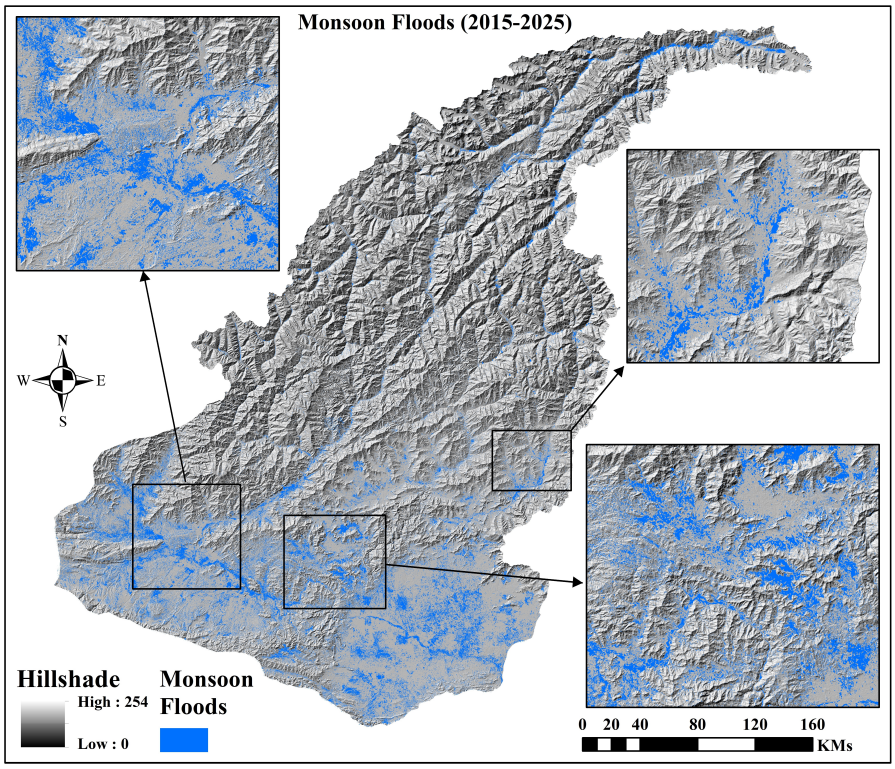


Figure 4. Integrated decadal map of monsoon flood in the KRB.

The highest classification performance was recorded in 2019, with an overall accuracy of 0.93 and a Kappa coefficient of 0.86, indicating very strong agreement. Similarly, 2015 and 2018 exhibited high reliability, with overall accuracy values above 0.90 and Kappa coefficients of 0.84. Slightly lower but still robust performance was observed in 2020 and 2025, with overall accuracy values of 0.87 and 0.86, respectively, and Kappa coefficients of 0.78 and 0.79 (Table 1). These minor reductions may reflect the increased complexity of large-magnitude flood events, heterogeneous land-cover conditions, and greater variability in radar backscatter. The absence of documented flood events in 2017 resulted in no classification assessment for that year.

Across the full study period, the integrated flood inundation map achieved an overall accuracy of 0.891 and a Kappa coefficient of 0.815 against the held-out pseudo-labeled samples. These results demonstrate consistent classification behavior relative to the high-confidence samples used for model development; however, they do not constitute an independent accuracy assessment because the pseudo-labels were generated from Sentinel-1 observations. In mountainous SAR-based flood mapping applications, values above 0.85 for overall accuracy and above 0.75 for Kappa are generally regarded as robust, particularly under complex topographic and hydrological conditions [1,30].

Furthermore, the final integrated decadal flood-inundation map was evaluated using receiver operating characteristic (ROC) analysis. The resulting AUC of 0.924 indicates strong discrimination between the flooded and non-flooded classes relative to the available reference samples. However, because the reference information was derived from Sentinel-1-based pseudo-labels, the ROC-AUC should be interpreted as an assessment of the model's discriminatory consistency rather than as an independent measure of absolute flood-mapping accuracy. An AUC exceeding 0.90 is widely considered indicative of very strong model performance in environmental remote sensing applications [21,31].

The ROC analysis also identified an optimal classification threshold based on Youden's J statistic. The maximum J value reached 0.712, indicating a well-balanced trade-off between sensitivity and specificity. This high J value confirms that the selected threshold maximizes true positive detection while minimizing false positives, thereby improving the reliability of the final binary flood mask. The position of the optimal J point on the ROC curve (Figure 5) further illustrates the ability of the adopted method to achieve high true positive rates at relatively low false positive rates, reinforcing the strong discriminatory power of the Random Forest classifier.

In addition to the internal statistical assessment, the mapped flood extents were independently cross-checked for spatial and hydrological plausibility against available flood inventories, cloud-free high-resolution optical imagery, documented flood reports, and available field observations. These independent sources were used as external evidence to examine whether the mapped inundation corresponded to known flood-affected areas, river corridors, downstream floodplains, and low-elevation flow-accumulation zones. Because these sources were not consistently available at comparable spatial and temporal resolution for all events, they were used for independent qualitative verification rather than calculation of event-specific accuracy metrics. The agreement observed across these independent sources provides supporting evidence for the spatial realism of the reconstructed inundation patterns, while the absence of a consistent independent reference dataset remains an important limitation.

Overall, the combined confusion matrix metrics, ROC analysis, and independent spatial validation demonstrate that the Sentinel-1 SAR and Random Forest framework provides reliable, consistent, and hydrologically meaningful flood delineation across the KRB.

Table 1. Annual and integrated inundated areas, overall accuracy and Kappa coefficient for flood inundation mapping in the KRB (2015–2025).

Flood	Inundation (Km^2)	Overall Accuracy	Kappa Coefficient
2015	420	0.92	0.84
2016	379	0.86	0.81
2017	0	-	-
2018	504	0.91	0.84
2019	627	0.93	0.86
2020	1004	0.87	0.78
2021	624	0.89	0.79
2022	688	0.91	0.83
2023	242	0.89	0.81
2024	466	0.87	0.8
2025	459	0.86	0.79
Integrated	4008	0.891	0.815

Note: After removing the overlap areas, the integrated maps show that a total of 4008 km^2 were inundated at least once in a decade. Furthermore, no flood was detected in 2017; therefore, OA and Kappa were not calculated for that year.

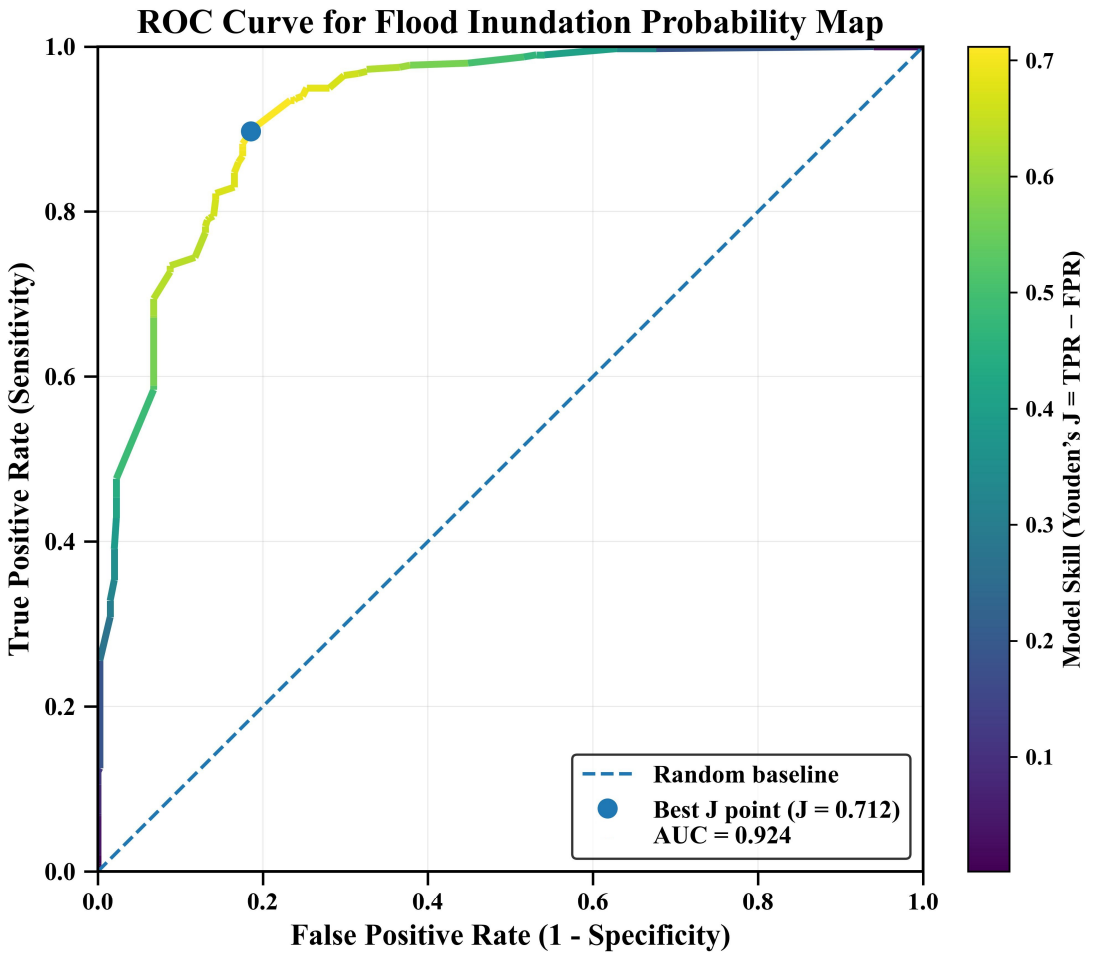


Figure 5. ROC curve of the integrated flood inundation probability map for the Kabul River Basin (2015–2025).

5. Discussion

The interannual flood inundation patterns derived from the Random Forest–based Sentinel-1 SAR analysis highlight substantial hydroclimatic variability in the KRB. The marked expansion of inundation in 2020 (1004 km^2), followed by relatively high inundation in 2021 (624 km^2) and 2022 (688 km^2), contrasts with the more moderate extents observed during 2015–2018 and the lower inundation recorded in 2023 (242 km^2). This variability is consistent with the hydroclimatic setting of the eastern Hindu Kush, where intense monsoon rainfall, antecedent catchment wetness, snowmelt and glacier-melt contributions, and complex topography interact to regulate runoff generation and flood propagation [1,26,32,33]. During periods of intense or persistent monsoon rainfall, wet antecedent conditions can reduce the basin's available storage capacity and enhance the conversion of rainfall into surface runoff, while snow and glacier melt provide an additional contribution to seasonal streamflow in the upper basin. In steep headwater regions, the combination of rainfall and cryospheric melt can produce rapid runoff concentration and rising discharge, which is then propagated toward wider downstream valleys and floodplains [3]. Once channel conveyance is exceeded, the relatively low-gradient downstream areas are more susceptible to overbank flow and prolonged inundation. Thus, large spatial differences in annual inundation reflect not only rainfall intensity but also the integrated influence of antecedent hydrological conditions, cryospheric contributions, drainage characteristics, and basin topography. Because this study reconstructs inundation from SAR observations rather than explicitly modelling rainfall–runoff or discharge, these hydroclimatic factors are interpreted as plausible controls on the observed temporal variability rather than quantitatively attributed to individual flood years [9,11].

The use of Sentinel-1 SAR proved particularly advantageous for capturing flood dynamics during peak monsoon periods, when optical imagery is often obstructed by persistent cloud cover. SAR backscatter reductions due to specular reflection over open water enabled reliable delineation of inundated surfaces even under adverse weather conditions, consistent with established SAR flood-detection principles [34,35]. However, flood mapping in mountainous terrain is complicated by terrain-induced distortions, incidence-angle effects, and heterogeneous land cover [11,36]. The incorporation of slope masking, permanent water exclusion based on long-term surface

water occurrence data, and orbit-consistent image selection helped mitigate these confounding factors, thereby enhancing the hydrological realism of the mapped inundation [24]. Compared with conventional threshold-based change detection, the Random Forest framework demonstrated greater flexibility and robustness in distinguishing flooded from non-flooded surfaces. The classifier captured nonlinear relationships between radar response and inundation processes. Random Forest, an ensemble learning structure that aggregates multiple decision trees trained on bootstrapped samples, reduces overfitting and improves generalization across heterogeneous landscapes [16,37]. The validation results for this study, with an AUC of 0.92, an average OA of 0.891, and a Cohen's Kappa coefficient of 0.815, indicate strong agreement between predicted and reference flood classes. These values fall within or above the performance ranges commonly reported for SAR-based RF flood mapping in complex environments, where OA typically exceeds 0.85, and Kappa values frequently range from 0.70 to 0.90 [11,38]. The achieved metrics confirm that the implemented preprocessing controls and feature engineering steps effectively reduced classification errors associated with terrain artefacts and background variability.

While Sentinel-1 SAR has become a widely adopted data source for flood inundation mapping, most previous studies have primarily relied on conventional change detection or threshold-based approaches for individual flood events. For example, recent studies conducted in Pakistan, including the application of the Change Detection Approach Technique (CDAT) in Google Earth Engine for flood mapping in Sindh Province and Sentinel-1A SAR-based flood assessment in the Indus River Basin, demonstrated the effectiveness of SAR imagery for rapid flood delineation during major flood events. These studies primarily focused on event-specific inundation extraction using backscatter differences and predefined thresholds [39]. Although such approaches are computationally efficient and suitable for emergency response, their performance can be affected by variations in acquisition geometry, land-cover heterogeneity, surface roughness, and complex topography, particularly when the same methodology is transferred across multiple flood events.

In contrast, the present study adopts a machine learning framework that extends beyond conventional SAR change detection by integrating orbit-consistent Sentinel-1 preprocessing, multi-temporal backscatter features, polarization information, GLCM texture descriptors, terrain variables, and pseudo-label-based Random Forest classification within a unified workflow. Rather than producing flood maps for a single event, the proposed framework was designed to reconstruct a temporally consistent decadal flood inventory spanning eleven monsoon seasons (2015–2025). The incorporation of pseudo-label generation further enables supervised learning in a data-scarce transboundary basin where reliable flood reference data are unavailable for most historical events. Consequently, the methodological contribution of this study lies not only in flood delineation itself but also in providing a transferable framework capable of generating consistent long-term flood inventories that support hydrological analysis, flood susceptibility assessment, and future risk modelling in mountainous regions.

The decade-scale cumulative inundation exceeding 4000 km^2 further emphasizes the recurrent nature of monsoon flooding in the KRB. Although a pixel-level flood-frequency or recurrence map would provide an additional means of identifying persistent flood-prone locations, such an analysis is beyond the primary scope of the present study, which focuses on reconstructing event-specific monsoon inundation and establishing a temporally consistent flood inventory for 2015–2025. Nevertheless, the annual inundation maps and the integrated decadal extent provide direct evidence of recurrent flooding, particularly across the downstream lowland floodplains and major river corridors. The resulting multi-year inventory can serve as the basis for a future frequency analysis in which the number of inundation occurrences at each pixel is explicitly quantified. Such a frequency-based product would be particularly useful for distinguishing persistent flood-prone areas from locations affected by isolated extreme events and could subsequently support spatial flood-hazard zoning and risk-management planning. Notably, except for 2017, the basin experienced measurable monsoon-related inundations each year during the study period, underscoring persistent hydrological exposure. While the present analysis focuses exclusively on monsoon floods, the region also experiences spring and winter flood events, suggesting that total annual flood exposure may be even greater than represented here [5]. The probability-based output of the RF model provides flexibility for future applications, including uncertainty analysis, threshold sensitivity assessment, and integration with flood susceptibility assessment.

Nevertheless, certain limitations should be acknowledged. First, because consistent event-specific ground-reference polygons are unavailable across the transboundary KRB, the RF models were trained and evaluated using high-confidence pseudo-labels derived from Sentinel-1 observations. Although the use of held-out pseudo-labels provides an internal assessment of classification consistency, it does not constitute a fully independent accuracy assessment and may result in optimistic performance estimates because the reference information and predictor variables originate from the same SAR data source. To partially address this limitation, the resulting inundation maps were additionally cross-checked against available independent flood inventories, cloud-free optical imagery, documented flood reports, and field observations. However, these sources were not sufficiently

consistent in spatial and temporal coverage to support a quantitative independent validation for every event. Future work should therefore prioritize systematic validation against independently derived flood products, such as Copernicus Emergency Management Service, UNOSAT, Sentinel-2-based reference maps, or official flood inventories, when temporally and spatially consistent datasets become available.

6. Conclusions

This study presented a decadal reconstruction of monsoon flood inundation in the Kabul River Basin (KRB) for the period 2015–2025 using a Sentinel-1 Synthetic Aperture Radar (SAR) dataset integrated with a Random Forest (RF) machine learning framework. The proposed methodology combined orbit-consistent SAR preprocessing, speckle filtering, terrain and permanent water masking, multi-temporal backscatter change metrics, polarization features, texture descriptors, and topographic variables to ensure robust flood detection in a complex mountainous environment. In the absence of consistent ground reference data, a pseudo-labeling strategy was employed to generate high-confidence training samples, enabling reliable event-based flood classification across multiple years.

The results demonstrate strong interannual variability in monsoon flood inundation across the basin. Moderate flood extents were observed during 2015–2018, while extreme inundation occurred in 2020 (1004 km^2), followed by persistently high flood activity during 2021–2022. In contrast, relatively lower inundation was recorded in 2023–2025. Except for 2017, flood events were detected every year, highlighting the recurrent nature of monsoon-driven hydrological hazards in the KRB. The cumulative inundated area exceeded 4000 km^2 over the study period, further emphasizing the basin's persistent flood exposure.

Model evaluation results showed strong internal agreement between the RF predictions and the held-out pseudo-labeled samples, with overall accuracy ranging from 0.86 to 0.93, Cohen's Kappa from 0.78 to 0.86, and an integrated ROC-AUC of 0.924. These results demonstrate consistent discriminatory performance of the proposed framework; however, because the reference samples were derived from Sentinel-1 observations, the reported metrics should not be interpreted as fully independent estimates of absolute mapping accuracy.

Beyond flood mapping, the generated inundation dataset makes a critical contribution to hydrological research by providing a temporally consistent, observation-based flood inventory. This dataset directly supports downstream applications, particularly flood susceptibility and risk modeling, ensuring that vulnerability assessments are grounded in empirically reconstructed flood events rather than sparse point-based records. Spatial analysis further confirms that flood inundation is predominantly concentrated in downstream lowland floodplains, reflecting strong geomorphological control over flood propagation.

Despite its strengths, the study acknowledges limitations associated with pseudo-label-based training, which may introduce uncertainty in areas with complex vegetation or mixed surface conditions. Future work could improve robustness by integrating hydrodynamic modeling outputs or by employing multi-sensor fusion approaches that combine SAR and optical datasets.

Overall, the proposed Sentinel-1 SAR and Random Forest framework extends conventional SAR change-detection approaches by integrating multi-feature machine learning, pseudo-label-based supervised training, and temporally consistent multi-event reconstruction within a unified workflow. The resulting decadal flood inventory provides a scalable and transferable foundation for flood susceptibility assessment, hydrological analysis, and flood-risk management in data-scarce mountainous basins.

Funding

This research received no external funding.

Institutional Review Board Statement

Not applicable.

Informed Consent Statement

Not applicable.

Data Availability Statement

Codes and other data will be available upon request.

Conflicts of Interest

The author declares no conflict of interest.

Use of AI and AI-Assisted Technologies

During the preparation of this work, the author used Grammarly and ChatGPT Plus for English proofreading. The authors take full responsibility for the content of the published article.

References

1. Rahman, Z.U.; Zhang, M.; Chen, F.; et al. Spatiotemporal dynamics of flood susceptibility under future precipitation variability, population growth, and land cover change. *Int. J. Appl. Earth Obs. Geoinf.* **2026**, *147*, 105193. https://doi.org/10.1016/j.jag.2026.105193.
2. Sadhwani, K.; Eldho, T.I. Machine Learning-Driven Flood Hazard Assessment: Integrating SAR and Elevation Data for Inundation Mapping and Depth Estimation. *Nat. Hazards* **2026**, *122*, 177. https://doi.org/10.1007/s11069-025-07949-y.
3. Rahman, Z.U.; Chen, F.; Zhang, M.; et al. Identification and mapping of multi-type flood hotspots using an ensemble technique in the transboundary of Kabul River Basin. *J. Hydrol. Reg. Stud.* **2025**, *60*, 102468. https://doi.org/10.1016/j.ejrh.2025.102468.
4. Hussain, M.; Tayyab, M.; Ullah, K.; et al. Development of a new integrated flood resilience model using machine learning with GIS-based multi-criteria decision analysis. *Urban Clim.* **2023**, *50*, 101589. https://doi.org/10.1016/j.uclim.2023.101589.
5. Rahman, Z.U.; Zhang, M.; Chen, F.; et al. Flood susceptibility mapping using supervised machine learning models: Insights into predictors' significance and models' performance. *Geomat. Nat. Hazards Risk* **2025**, *16*, 2516728. https://doi.org/10.1080/19475705.2025.2516728.
6. Ullah, M.; Wang, C.; Ullah, S.; et al. Summer monsoon precipitation patterns and their relationship to flood probabilities across Pakistan. *J. Hydrol. Reg. Stud.* **2026**, *65*, 103485. https://doi.org/10.1016/j.ejrh.2026.103485.
7. Gao, D.; Wang, W.; Yin, J.; et al. Validation of flood inundation modelling using multi-source SAR imagery. *Water Res.* **2026**, *296*, 125590. https://doi.org/10.1016/j.watres.2026.125590.
8. Sharma, N.K.; Saharia, M. DeepSARFlood: Rapid and automated SAR-based flood inundation mapping using vision transformer-based deep ensembles with uncertainty estimates. *Sci. Remote Sens.* **2025**, *11*, 100203. https://doi.org/10.1016/j.srs.2025.100203.
9. Li, Y.; Martinis, S.; Plank, S.; et al. An automatic change detection approach for rapid flood mapping in Sentinel-1 SAR data. *Int. J. Appl. Earth Obs. Geoinf.* **2018**, *73*, 123–135. https://doi.org/10.1016/j.jag.2018.05.023.
10. Arora, M.; Sahoo, S.; Bhatt, C.M.; et al. Rapid flood inundation mapping and impact assessment using Sentinel-1 SAR data over Ghaggar River basin of Punjab, India. *J. Earth Syst. Sci.* **2023**, *132*, 183. https://doi.org/10.1007/s12040-023-02199-7.
11. Halder, K.; Ghosh, A.; Srivastava, A.K.; et al. SAR-driven flood inventory and multi-factor ensemble susceptibility modelling using machine learning frameworks. *Geomat. Nat. Hazards Risk* **2024**, *15*, 2409202. https://doi.org/10.1080/19475705.2024.2409202.
12. Tavus, B.; Kocaman, S. Flood Mapping in Mountainous Areas Using Sentinel-1 & 2 Data and GLCM Features. *Int. Arch. Photogramm. Remote Sens. Spat. Inf. Sci.* **2023**, *48*, 1575–1580. https://doi.org/10.5194/isprs-archives-xlviii-1-w2-2023-1575-2023.
13. Jishnu, V.; Arora, M.; Singh, H.; et al. Flood Inundation Mapping Over Kerala Region During 2018 Flood—Based on Cloud Computing and Automatic Threshold Detection Approach. In *Climate, Environment and Agricultural Development*; Springer Nature: Singapore, 2024; pp. 145–165.
14. Arora, M.; Setia, R.; Singh, R.; et al. Mapping of Flood Inundated Areas Using Earth Observation Data and Cloud Computing Platform. *J. Atmos. Sol.-Terr. Phys.* **2025**, *274*, 106567.
15. Zhou, C.; Wu, W.; Ke, X.; et al. Assessment of flooding and drought disaster risk in Henan, China by a multiscale approach. *Geomat. Nat. Hazards Risk* **2025**, *16*, 2491474. https://doi.org/10.1080/19475705.2025.2491474.
16. Misra, A.; White, K.; Nsutezo, S.F.; et al. Mapping Global Floods with 10 Years of Satellite Radar Data. *Nat. Commun.* **2025**, *16*, 5762.
17. Breiman, L. Random Forests. *Mach. Learn.* **2001**, *45*, 5–32. https://doi.org/10.1023/a:1010933404324.
18. Jiao, Z.; Zhang, Z.; Wu, L. SAR-based dynamic information retrieving of the Beijing-Tianjin-Hebei flood-inundation happened in July 2023, North China. *Geomat. Nat. Hazards Risk* **2024**, *15*, 2366361. https://doi.org/10.1080/19475705.2024.2366361.
19. Irukumati, S.; Vittal, A.R.; Gurunarayan, S.L. Comparative analysis of classification techniques for flood mapping using Sentinel 1 SAR data. *Environ. Earth Sci.* **2025**, *84*, 398. https://doi.org/10.1007/s12665-025-12381-3.

20. Subramonian, K.; Girisha, S.; Savitha, G.; et al. Ensemble Teacher Models for Semi-Supervised Semantic Segmentation of Flood Zones from Synthetic Aperture Radar Images. *Multimed. Tools Appl.* **2026**, *85*, 308. https://doi.org/10.1007/s11042-026-21500-6.
21. Savitha, G.; Girisha, S.; Sughosh, P.; et al. Consistency Regularization for Semi-Supervised Semantic Segmentation of Flood Regions from SAR Images. *IEEE Access* **2025**, *13*, 9642–9653. https://doi.org/10.1109/access.2025.3526244.
22. Lashkaripour, G.R.; Hussaini, S.A. Water Resource Management in Kabul River Basin, Eastern Afghanistan. *Environ.* **2008**, *28*, 253–260. https://doi.org/10.1007/s10669-007-9136-2.
23. Khatiwada, K.R.; Pradhananga, S.; Nepal, S. Inferring the impacts of climate extreme in the Kabul River Basin. *Reg. Environ. Chang.* **2024**, *24*, 17. https://doi.org/10.1007/s10113-023-02167-3.
24. Sayama, T.; Ozawa, G.; Kawakami, T.; et al. Rainfall–Runoff–Inundation Analysis of the 2010 Pakistan Flood in the Kabul River Basin. *Hydrol. Sci. J.* **2012**, *57*, 298–312. https://doi.org/10.1080/02626667.2011.644245.
25. Ullah, W.; Wang, G.; Lou, D.; et al. Large-Scale Atmospheric Circulation Patterns Associated with Extreme Monsoon Precipitation in Pakistan during 1981–2018. *Atmos. Res.* **2021**, *253*, 105489. https://doi.org/10.1016/j.atmosres.2021.105489.
26. Rahman, Z.U.; Ullah, W.; Bai, S.; et al. GIS-Based Flood Susceptibility Mapping Using Bivariate Statistical Model in Swat River Basin, Eastern Hindukush Region, Pakistan. *Front. Environ. Sci.* **2023**, *11*, 1178540. https://doi.org/10.3389/fenvs.2023.1178540.
27. Moorthy, R.; Bibi, S. Water Security and Cross-Border Water Management in the Kabul River Basin. *Sustainability* **2023**, *15*, 792. https://doi.org/10.3390/su15010792.
28. Ougahi, J.H.; Karim, S.; Mahmood, S.A. Application of the SWAT model to assess climate and land use/cover change impacts on water balance components of the Kabul River Basin, Afghanistan. *J. Water Clim. Chang.* **2022**, *13*, 3977–3999. https://doi.org/10.2166/wcc.2022.261.
29. Shams, A.K.; Muhammad, N.S. Towards Sustainable Transboundary Water Cooperation between Afghanistan and Pakistan: A Case Study of Kabul River. *Ain Shams Eng. J.* **2023**, *14*, 101842. https://doi.org/10.1016/j.asej.2022.101842.
30. Baig, S.; Hasson, S.U. Flood Inundation and Streamflow Changes in the Kabul River Basin under Climate Change. *Sustainability* **2023**, *16*, 116. https://doi.org/10.3390/su16010116.
31. Hussain, M.; Ullah, K.; Tayyab, M.; et al. Data-driven multi-hazard susceptibility and community perceptions assessment using a mixed-methods approach. *J. Environ. Manag.* **2025**, *388*, 126009. https://doi.org/10.1016/j.jenvman.2025.126009.
32. Hashmi, M.Z.U.R.; Masood, A.; Mushtaq, H.; et al. Exploring climate change impacts during first half of the 21st century on flow regime of the transboundary Kabul River in the Hindukush region. *J. Water Clim. Chang.* **2020**, *11*, 1521–1538. https://doi.org/10.2166/wcc.2019.094.
33. Torres, R.; Snoeij, P.; Geudtner, D.; et al. GMES Sentinel-1 mission. *Remote Sens. Environ.* **2012**, *120*, 9–24. https://doi.org/10.1016/j.rse.2011.05.028.
34. Pulvirenti, L.; Pierdicca, N.; Chini, M.; et al. An Algorithm for Operational Flood Mapping from Synthetic Aperture Radar (SAR) Data Using Fuzzy Logic. *Nat. Hazards Earth Syst. Sci.* **2011**, *11*, 529–540. https://doi.org/10.5194/nhess-11-529-2011.
35. Martinis, S.; Kersten, J.; Twele, A. A Fully Automated TerraSAR-X Based Flood Service. *ISPRS J. Photogramm. Remote Sens.* **2015**, *104*, 203–212. https://doi.org/10.1016/j.isprsjprs.2014.07.014.
36. Zhu, Z.; Zhang, Y. Flood disaster risk assessment based on random forest algorithm. *Neural Comput. Appl.* **2022**, *34*, 3443–3455. https://doi.org/10.1007/s00521-021-05757-6.
37. Tayyab, M.; Zhang, J.; Hussain, M.; et al. GIS-Based Urban Flood Resilience Assessment Using Urban Flood Resilience Model: A Case Study of Peshawar City, Khyber Pakhtunkhwa, Pakistan. *Remote Sens.* **2021**, *13*, 1864. https://doi.org/10.3390/rs13101864.
38. Mehmood, Z.; Rahman, G. Assessing Flood Inundation and its impacts Using Sentinel-1A SAR Data and the Sentinel Application Platform in the Indus River Basin. *Ecol. Quest.* **2026**, *37*, 1–33. https://doi.org/10.12775/eq.2026.027.
39. Ghouri, A.Y.; ur Rehman, A.; Rasheed, F.; et al. Flood Mapping Using the Sentinel-1 SAR Dataset and Application of the Change Detection Approach Technique (CDAT) to the Google Earth Engine in Sindh Province, Pakistan. *Ecol. Quest.* **2024**, *35*, 149–159.